Hindawi Publishing Corporation
EURASIP Journal on Wireless Communications and Networking
Volume 2010, Article ID 523435, 8 pages
doi:10.1155/2010/523435

Research Article

Biologically Inspired Target Recognition in Radar Sensor Networks

Qilian Liang

Department of Electrical Engineering, University of Texas at Arlington, Arlington, TX 76019-0016, USA

Correspondence should be addressed to Qilian Liang, liang@uta.edu

Received 10 September 2009; Accepted 9 November 2009

Academic Editor: Benyuan Liu

Copyright © 2010 Qilian Liang. This is an open access article distributed under the Creative Commons Attribution License, which permits unrestricted use, distribution, and reproduction in any medium, provided the original work is properly cited.

One of the great mysteries of the brain is cognitive control. How can the interactions between millions of neurons result in behavior that is coordinated and appears willful and voluntary? There is consensus that it depends on the prefrontal cortex (PFC). Many PFC areas receive converging inputs from at least two sensory modalities. Inspired by human's innate ability to process and integrate information from disparate, network-based sources, we apply human-inspired information integration mechanisms to target detection in cognitive radar sensor network. Humans' information integration mechanisms have been modelled using maximum-likelihood estimation (MLE) or soft-max approaches. In this paper, we apply these two algorithms to cognitive radar sensor networks target detection. Discrete-cosine-transform (DCT) is used to process the integrated data from MLE or soft-max. We apply fuzzy logic system (FLS) to automatic target detection based on the AC power values from DCT. Simulation results show that our MLE-DCT-FLS and soft-max-DCT-FLS approaches perform very well in the radar sensor network target detection, whereas the existing 2D construction algorithm does not work in this study.

1. Introduction and Motivation

Humans display a remarkable capability to perform visual and auditory information integration despite noisy sensory signals and conflicting inputs. Humans are adept at network visualization, and at understanding subtle implications among the network connections. To date, however, human's innate ability to process and integrate information from disparate, network-based sources has not translated well to automated systems. Motivated by the above challenges, we apply human information integration mechnisms to cognitive radar sensor networks. A cognitive network is one that is aware of changes in user needs and its environment, adapts its behavior to those changes, learns from its adaptations, and exploits knowledge to improve its future behavior. A cognitive radar sensor network consists of multiple networked radar sensors and radar sensors sense and communicates with each other collaboratively to complete a mission. In real world, cognitive radar sensor network information integration is necessary in different applications. For example, in an emergency natural disaster scenario, such as China Wenchuan earthquake in May 2008, Utah Mine Collapse in August 2007, or West Virginia Sago mine disaster in January 2006, cognitive radar sensor network-based information integration for first responders is critical for search and rescue. Danger may appear anywhere at any time; therefore, first responders must monitor a large area continuously in order to identify potential danger and take actions. Due to the dynamic and complex nature of natural disaster, some buried/foleage victims may not be found with image/video sensors, and UWB radar sensors are needed for penetrating the ground or sense-through-wall. Unfortunately, the radar data acquired are often limited and noisy. Unlike medical imaging or synthetic aperture radar imaging where abundance of data is generally available through multiple looks and where processing time may not be crucial, practical cognitive radar sensor networks are typically the opposite: availability of data is limited and required processing time is short. This need is also motivated by the fact that humans display a remarkable capability to quickly perform target recognition despite noisy sensory signals and conflicting inputs. Humans are adept at network visualization and at understanding subtle implications among the network connections. To date, however, human's innate

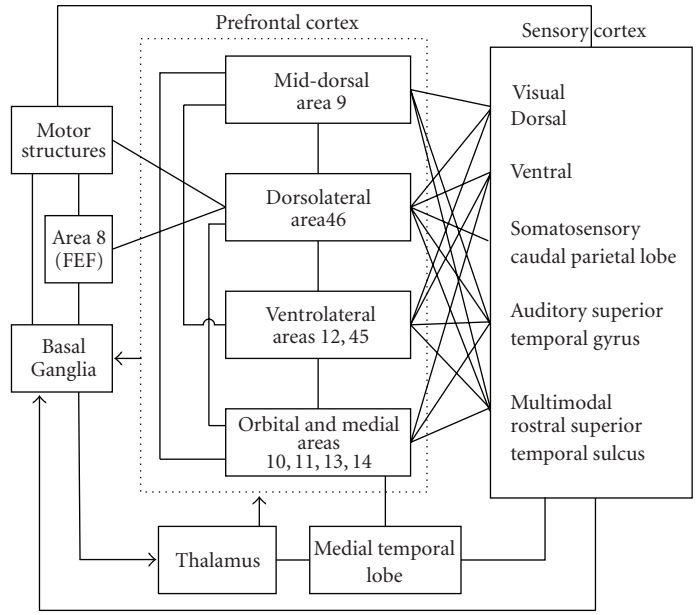

Figure 1: Schematic diagram of some of the extrinsic and intrinsic connections of the PFC. Most connections are reciprocal; the exceptions are indicated by arrows. The frontal eye field (FEF) has variously been considered either adjacent to or part of the PFC.

ability to process and integrate information from disparate, network-based sources for situational understanding has not translated well to automated systems. In this paper, we apply human information integration mechanisms to information fusion in cognitive radar sensor network.

The rest of this paper is organized as follows. In Section 2, we introduce the human information integration mechanisms and their mathematical modeling. In Section 3, we introduce the radar sensor network data collection. In Section 4, we apply the human information integration mechanisms to cognitive radar sensor network. In Section 5, we apply fuzzy logic system for target detection as a postprocessing for Section 4. In Section 6, we conclude this paper.

2. Human Information Integration Mechanisms

One of the great mysteries of the brain is cognitive control. How can the interactions between millions of neurons result in behavior that is coordinated and appears willful and voluntary? There is consensus that it depends on the prefrontal cortex (PFCs) [1, 2]. A schematic diagram of some of the extrinsic and intrinsic connections of the PFC is depicted in Figure 1 [1]. Many PFC areas receive converging inputs from at least two sensory modalities [3, 4]. For example, the dorsolateral (DL) (areas 8, 9, and 46) and ventrolateral (12 and 45) PFCs both receive projections from visual, auditory, and somatosensory cortex. Furthermore, the PFC is connected with other cortical regions that are themselves sites of multimodal convergence. Many PFC areas (9, 12, 46, and 45) receive inputs from the rostral superior temporal sulcus, which has neurons with bimodal or trimodal (visual, auditory, and somatosensory) responses [5, 6]. The arcuate sulcus region (areas 8 and 45) and area 12 seem to be particularly multimodal. They contain zones that receive overlapping inputs from three sensory modalities [6]. Observe, for example, that mid-dorsal area 9 directly processes and integrates visual, auditory, and multimodal information. Regarding the functional model/mechanisms of different PFC areas (in Figure 1): mid-dorsal area 9, dorsolateral area 46, and ventrolateral areas 12, 45, and orbital and medial areas 10, 11, 13, 14, different models and rules have been reported in the literature [7–10].

Recently, a maximum-likelihood estimation (MLE) approach was proposed for multisensory data fusion in human [7]. In the MLE approach [7], sensory estimates of an environmental property can be represented by $\hat{S}_j = f_i(S)$ where S is the physical property being estimated, f is the operation the nervous system performs to derive the estimate, and $\hat{S}$ is the perceptual estimate. Sensory estimates are subject to two types of error: random measurement error and bias. Thus, estimates of the same object property from different cues usually differ. To reconcile the discrepancy, the nervous system must either combine estimates or choose one, thereby ignoring the other cues. Assuming that each single-cue estimate is unbiased but corrupted by independent Gaussian noise, the statistically optimal strategy for cue combination is a weighted average [7]:

$$\hat{S}_c = \sum_{i=1}^{M} w_i \hat{S}_i, \tag{1}$$

where $w_i = (1/\sigma_i^2)/(\sum_j 1/\sigma_j^2)$ and is the weight given to the ith single-cue estimate, σ_i^2 is that estimates variance, and M is the total number of cues. Combining estimates by this MLE rule yields the least variable estimate of S and thus more precise estimates of object properties.

Besides, some other summation rules have been proposed in perception and cognition such as soft-max rule: $y = (\sum_{i=1}^{M} x_i^n)^{1/n}$ [10] where x_i denotes the input from an input source i, and M is the total number of sources. In this paper, we will apply MLE and soft-max human brain information integration mechanisms to cognitive radar sensor network information integration.

3. Radar Sensor Networks Data Measurement and Collection

Our work is based on the sense-through-foliage UWB radar sensor networks. The foliage experiment was constructed on a seven-ton man lift, which had a total lifting capacity of 450 kg. The limit of the lifting capacity was reached during the experiment as essentially the entire measuring apparatus was placed on the lift (as shown in Figure 2). The principle pieces of equipment secured on the lift are Barth pulser, Tektronix model 7704 B oscilloscope, dual antenna mounting stand, two antennas, rack system, IBM laptop, HP signal Generator, Custom RF switch and power supply, and Weather shield (small hut). The target is a trihedral reflector (as shown in Figure 3). Throughout this work, a Barth pulse source (Barth Electronics, Inc. model 732 GL) was used. The pulse generator uses a coaxial reed switch to discharge a charge line for a very fast rise time pulse outputs. The model 732 pulse generator provides pulses of less than 50 picoseconds (ps) rise time, with amplitude from 150 V to greater than 2 KV into any load impedance through a 50 ohm coaxial line. The generator is capable of producing pulses with a minimum width of 750 ps and a maximum of 1 microsecond. This output pulse width is determined by charge line length for rectangular pulses or by capacitors for 1/e decay pulses.

For the data we used in this paper, each sample is spaced at 50 picosecond interval, and 16000 samples were collected for each collection for a total time duration of 0.8 microsecond at a rate of approximately 20 Hz. We plot the transmitted pulse (one realization) in Figure 4(a) and the received echos in one collection in Figure 4(b) (averaged over 35 pulses). The data collections were extensive. 20 different positions were used, and 35 collections were performed at each position using UWB radar sensor networks.

Figure 2: This figure shows the lift with the experiment. The antennas are at the far end of the lift from the viewer under the roof that was built to shield the equipment from the elements. This picture was taken in September with the foliage largely still present. The cables coming from the lift are a ground cable to an earth ground and one of 4 tethers used in windy conditions.

Figure 3: The target (a trihedral reflector) is shown on the stand at 300 feet from the lift.

4. Human-Inspired Sense-through-Foliage Target Detection

In Figures 5(a) and 5(b), we plot two collections of UWB radars. Figure 5(a) has no target on range, and Figure 5(b) has target at samples around 13900. We plot the echo differences between Figures 5(a) and 5(b) in Figure 5(c). However, it is impossible to identify whether there is any target and where there is target based on Figure 5(c). Since significant pulse-to-pulse variability exists in the echos, this motivates us to explore the spatial and time diversity using Radar Sensor Networks (RSNs).

In RSN, the radar sensors are networked together in an ad hoc fashion. They do not rely on a preexisting fixed infrastructure, such as a wireline backbone network or a base station. They are self-organizing entities that are deployed on demand in support of various events surveillance, battlefield, disaster relief, search and rescue, and so forth. Scalability concern suggests a hierarchical organization of radar sensor networks with the lowest level in the hierarchy being a cluster. As argued in [11–14], in addition to helping with scalability and robustness, aggregating sensor nodes into clusters has additional benefits:

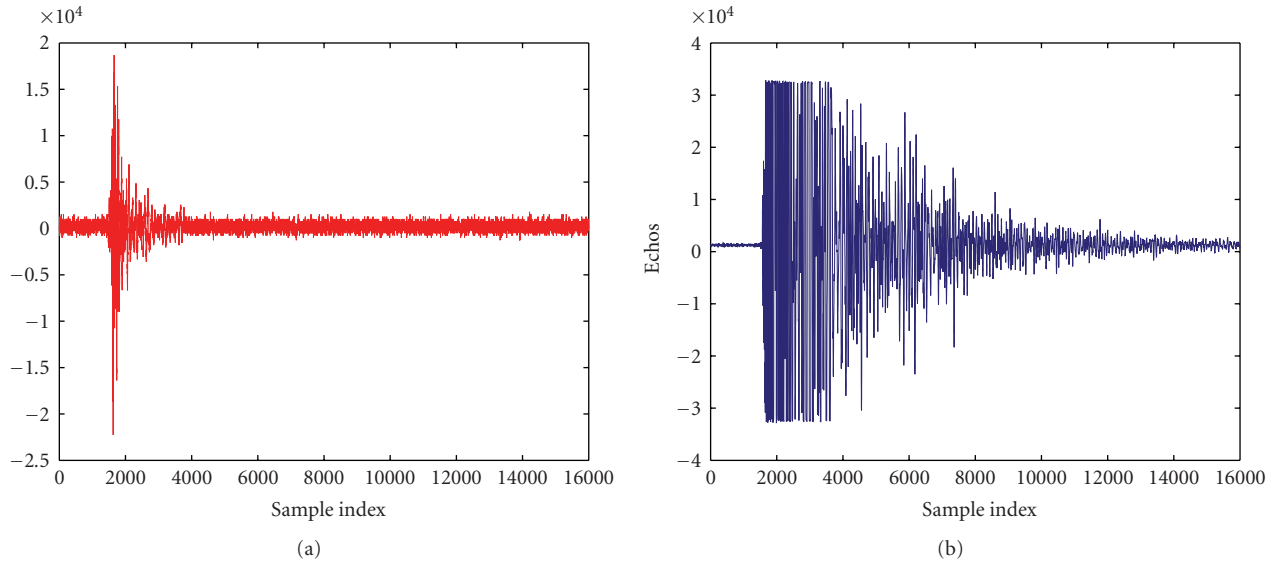

Figure 4: Transmitted pulse and received echos in one experiment. (a) Transmitted pulse. (b) Received echos.

(1) conserving radio resources such as bandwidth;

(2) promoting spatial code reuse and frequency reuse;

(3) simplifying the topology, for example, when a mobile radar changes its location, it is sufficient for only the nodes in attended clusters to update their topology information;

(4) reducing the generation and propagation of routing information;

(5) concealing the details of global network topology from individual nodes.

In RSN, each radar can provide their pulse parameters such as timing to their clusterhead radar, and the clusterhead radar can combine the echos (RF returns) from the target and clutter. In this paper, we propose an RAKE structure for combining echos, as illustrated by Figure 6. The integration means time-average for a sample duration T and it is for general case when the echos are not in discrete values. It is quite often assumed that the radar sensor platform will have access to Global Positioning Service (GPS) and Inertial Navigation Unit (INU) timing and navigation data [15]. In this paper, we assume that the radar sensors are synchronized in RSN. In Figure 6, the echo, that is, RF response by the pulse of each cluster-member sensor, will be combined by the clusterhead using a weighted average, and the weight w_i is determined by the two human-inspired mechanisms.

We applied the human-inspired MLE algorithm to combine the sensed echo collection from $M = 30$ UWB radars, and then the combined data are processed using discrete-cosine transform (DCT) to obtain the AC values. Based on our experiences, echo with a target generally has high and nonfluctuating AC values and the AC values can be obtained using DCT. We plot the power of AC values in Figures 7(a) and 7(b) using MLE and DCT algorithms for the two cases (with target and without target), respectively. Observe that in Figure 7(b) the power of AC values (around sample 13900) where the target is located is nonfluctuating (somehow monotonically increase then decrease). Although some other samples also have very high AC power values, it is very clear that they are quite fluctuating and the power of AC values behaves like random noise because generally the clutter has Gaussian distribution in the frequency domain.

Similarly, we applied the soft-max algorithm ($n = 2$) to combine the sensed echo collection from $M = 30$ UWB radars, and then used DCT to obtain the AC values. We plot the power of AC values in Figures 7(a) and 7(b) using soft-max and DCT algorithms for the two cases (with target and without target) respectively. Observe that in Figure 8(b), the power of AC values (around sample 13,900) where the target is located is nonfluctuating (somehow monotonically increase then decrease).

We made the above observations. However, in real world application, automatic target detection is necessary to ensure that our algorithms could be performed in real time. In Section 5, we apply fuzzy logic systems to automatic target detection based on the power of AC values (obtained via MLE-DCT or soft-max-DCT).

We compared our approaches to the scheme proposed in [16]. In [16], 2D image was created via adding voltages with the appropriate time offset. In Figures 9(a) and 9(b), we plot the 2D image created based on the above two data sets (from samples 13800 to 14200). The sensed data from 30 radars are averaged first and then plotted in 2D [16]. However, it is not clear which image shows there is target on range.

5. Fuzzy Logic System for Automatic Target Detection

5.1. Overview of Fuzzy Logic Systems. Figure 10 shows the structure of a fuzzy logic system (FLS) [17]. When an input is

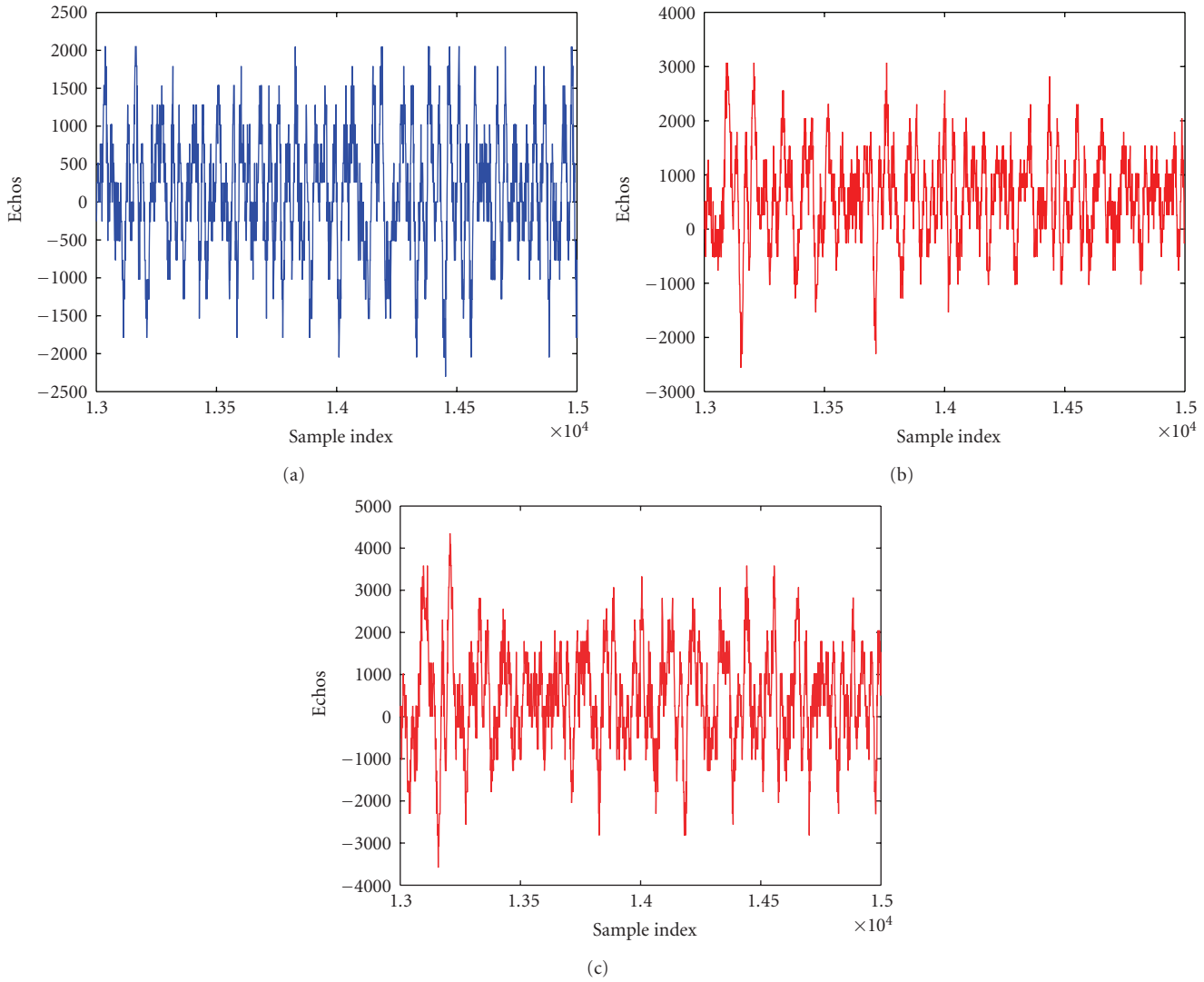

Figure 5: Measurement with 35 pulses average. (a) Expanded view of traces (no target) from sample 13001 to 15000. (b) Expanded view of traces (with target) from samples 13001 to 15000. (c) The differences between (a) and (b).

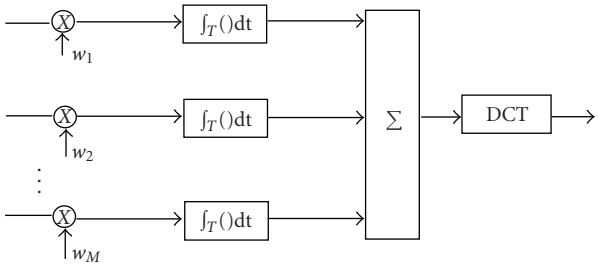

Figure 6: Echo combining by clusterhead in RSN.

applied to an FLS, the inference engine computes the output set corresponding to each rule. The defuzzifer then computes a crisp output from these rule output sets. Consider a p-input 1-output FLS, using singleton fuzzification, *center-of-sets* defuzzification [17], and "IF-THEN" rules of the form

$$R^l: \text{IF } x_1 \text{ is } F_1^l \text{ and } x_2 \text{ is } F_2^l \text{ and } \cdots \text{ and } x_p \text{ is } F_p^l, \text{ THEN } y \text{ is } G^l.$$

Assuming singleton fuzzification, when an input $\mathbf{x}' = \{x_1', \ldots, x_p'\}$ is applied, the degree of firing corresponding to the lth rule is computed as

$$\mu_{F_1^l}(x_1') \star \mu_{F_2^l}(x_2') \star \cdots \star \mu_{F_p^l}(x_p') = \mathcal{T}_{i=1}^{p} \mu_{F_i^l}(x_i'), \quad (2)$$

where $\star$ and $\mathcal{T}$ both indicate the chosen t-norm. There are many kinds of defuzzifiers. In this paper, we focus, for illustrative purposes, on the center-of-sets defuzzifier [17]. It computes a crisp output for the FLS by first computing the centroid, c_{G^l}, of every consequent set G^l, and then computing a weighted average of these centroids. The weight corresponding to the lth rule consequent centroid is the

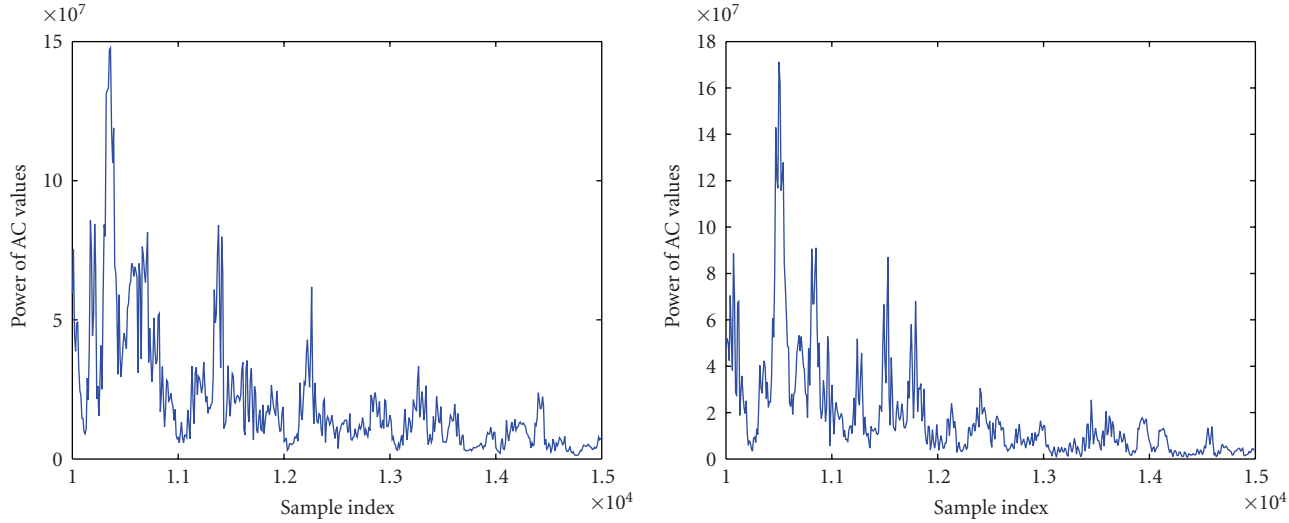

Figure 7: Power of AC values using MLE-based information integration and DCT. (a) No target (b) With target in the field.

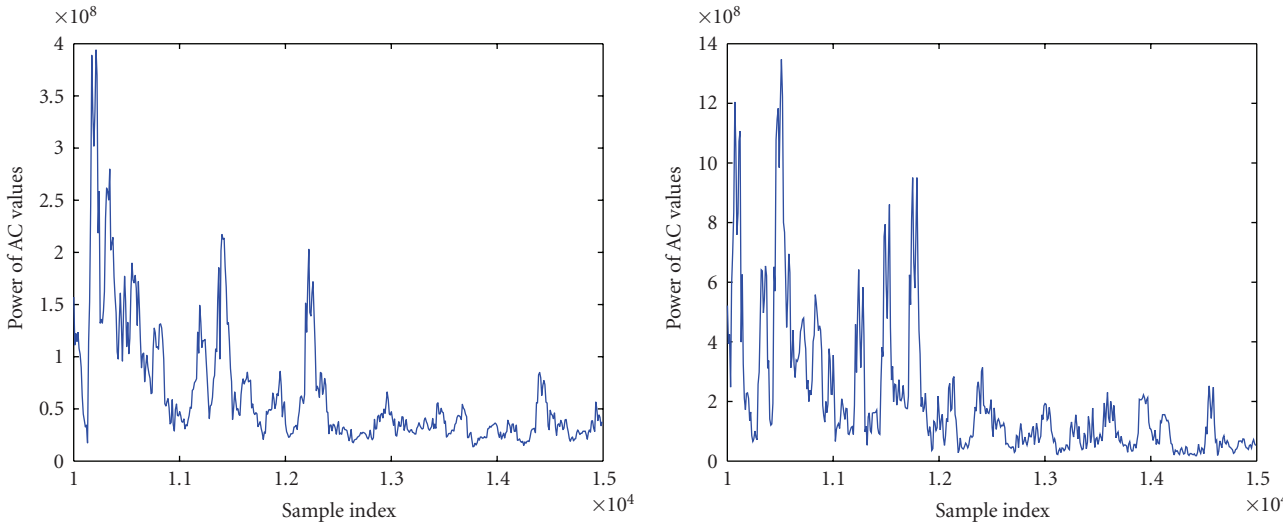

Figure 8: Power of AC values using soft-max-based information integration and DCT. (a) No target (b) With target in the field.

degree of firing associated with the lth rule, $\mathcal{T}_{i=1}^{p}\mu_{F_i^l}(x_i')$, so that

$$y_{\cos}(\mathbf{x}') = \frac{\sum_{l=1}^{M} c_{G^l}\mathcal{T}_{i=1}^{p}\mu_{F_i^l}(x_i')}{\sum_{l=1}^{M}\mathcal{T}_{i=1}^{p}\mu_{F_i^l}(x_i')}, \tag{3}$$

where M is the number of rules in the FLS. In this paper, we design an FLS for automatic target recognition based on the AC values obtained using MLE-DCT or soft-max-DCT.

5.2. FLS for Automatic Target Detection. Observe that, in Figures 7 and 8, the power of AC values are quite fluctuating and have lots of uncertainties. FLS is well known to handle the uncertainties. For convenience in describing the FLS design for Automatic Target Detection (ATD), we first give the definition of *footprint of uncertainty* of AC power values and *region of interest* in the footprint of uncertainty.

Definition 1 (*Footprint of Uncertainty*). Uncertainty in the AC power values and time index consists of a bounded region, that we call the *footprint of uncertainty* of AC power values. It is the union of all AC power values.

Definition 2 (*Region of Interest (RoI)*). An RoI in the footprint of uncertainty is a contour consisting of a large number (greater than 50) of AC power values where AC power values increase and then decrease.

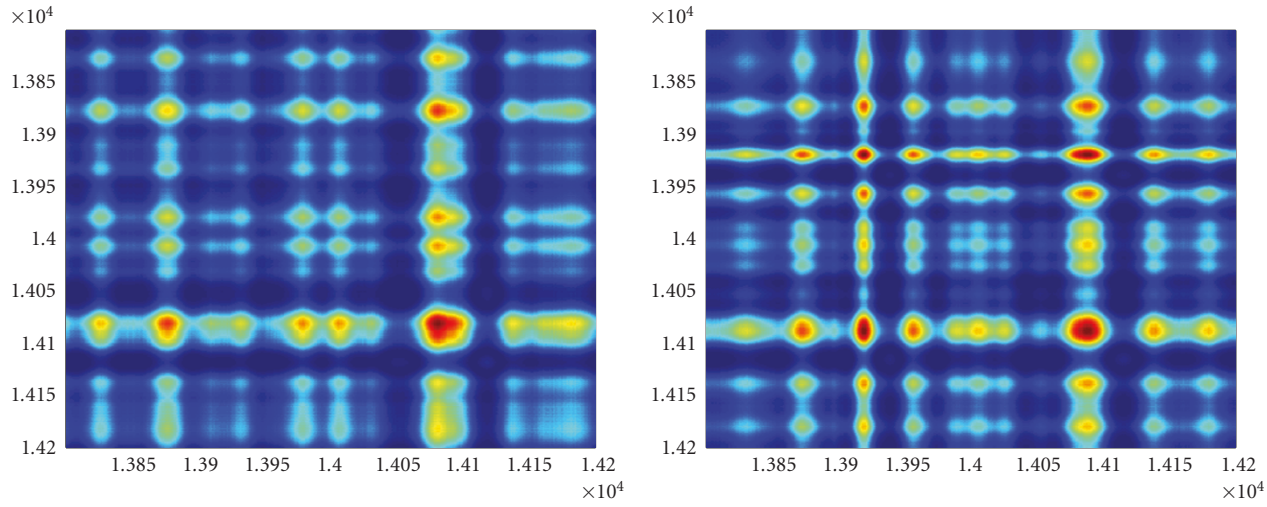

Figure 9: 2-D image created via adding voltages with the appropriate time offset. (a) No target (b) With target in the field.

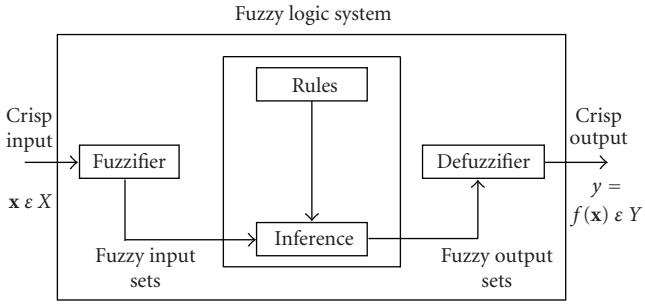

Figure 10: The structure of a fuzzy logic system.

Definition 3 (*Fluctuating Point in RoI*). $P(i)$ is called a *fluctuating point* in the RoI if $P(i-1), P(i), P(i+1)$ are nonmonotonically increasing or decreasing.

Our FLS for automatic target detection will classify each ROI (with target or no target) based on two antecedents: *the centroid of the ROI* and *the number of fluctuating points in the ROI*. The linguistic variables used to represent these two antecedents were divided into three levels: *low*, *moderate*, and *high*. The consequent—the possibility that there is a target at this RoI—was divided into 5 levels, *Very Strong, Strong, Medium, Weak,* and *Very Weak*. We used trapezoidal membership functions (MFs) to represent *low*, *high*, *very strong*, and *very weak* and triangle MFs to represent *moderate*, *strong*, *medium*, and *weak*. All inputs to the antecedents are normalized to 0–10.

Based on the fact the AC power value of target is nonfluctuating (somehow monotonically increase then decrease), and the AC power value of clutter behaves like random noise because generally the clutter has Gaussian distribution in the frequency domain, we design a fuzzy logic system using rules such as

Table 1: The rules for target detection. Antecedent 1 is *centroid of a RoI*, Antecedent 2 is *the number of fluctuating points in the ROI*, and Consequent is *the possibility that there is a target at this RoI*.

Rule number	Antecedent 1	Antecedent 2	Consequent
1	low	low	medium
2	low	moderate	weak
3	low	high	very weak
4	moderate	low	strong
5	moderate	moderate	medium
6	moderate	high	weak
7	high	low	very strong
8	high	moderate	strong
9	high	high	medium

R^l : IF *centroid of a RoI* (x_1) is F_l^1, and *the number of fluctuating points in the ROI* (x_2) is F_l^2, THEN the possibility that there is a target at this RoI (y) is G^l,

where $l = 1, \ldots, 9$. We summarize all the rules in Table 1. For every input (x_1, x_2), the output is computed using

$$y(x_1, x_2) = \frac{\sum_{l=1}^{9} \mu_{F_l^1}(x_1)\mu_{F_l^2}(x_2)c_{\text{avg}}^l}{\sum_{l=1}^{9} \mu_{F_l^1}(x_1)\mu_{F_l^2}(x_2)}. \quad (4)$$

We ran simulations to 1000 collections in the real world sense-through-foliage experiment and found that our FLS performs very well in the automatic target detection based on the AC power values obtained from MLE-DCT or soft-max-DCT and achieve probability of detection $p_d = 100\%$ and false alarm rate $p_{fa} = 0$.

6. Conclusions

Inspired by human's innate ability to process and integrate information from disparate, network-based sources, we applied human-inspired information integration mechanisms to target detection in cognitive radar sensor network. Humans' information integration mechanisms have been modelled using maximum-likelihood estimation (MLE) or soft-max approaches. In this paper, we applied these two algorithms to cognitive radar sensor networks target detection. Discrete-cosine-transform (DCT) was used to process the integrated data from MLE or soft-max. We applied fuzzy logic system (FLS) to automatic target detection based on the AC power values from DCT. Simulation results showed that our MLE-DCT-FLS and soft-max-DCT-FLS approaches performed very well in the radar sensor network target detection, whereas the existing 2-D construction algorithm could not work in this study.

Acknowledgments

The author would like to thank Dr. Sherwood W. Samn in AFRL/RHX for providing the radar data. This work was supported in part by the U.S. Office of Naval Research (ONR) under Grants N00014-07-1-0395, N00014-07-1-1024, and N00014-03-1-0466 and the National Science Foundation (NSF) under Grants CNS-0721515, CNS-0831902, and CCF-0956438. Some material in this paper has been presented at International Conference on Wireless Algorithms, Systems, and Applications, August 2009, Boston, MA.

References

[1] E. K. Miller and J. D. Cohen, "An integrative theory of prefrontal cortex function," *Annual Review of Neuroscience*, vol. 24, pp. 167–202, 2001.

[2] R. C. O'Reilly, "Biologically based computational models of high-level cognition," *Science*, vol. 314, no. 5796, pp. 91–94, 2006.

[3] D. A. Chavis and D. N. Pandya, "Further observations on cortico-frontal connections in the rhesus monkey," *Brain Research*, vol. 117, pp. 369–386, 1976.

[4] E. G. Jones and T. P. Powell, "An anatomical study of converging sensory pathways within the cerebral cortex of the monkey," *Brain*, vol. 93, no. 4, pp. 793–820, 1970.

[5] C. Bruce, R. Desimone, and C. G. Gross, "Visual properties of neurons in a polysensory area in superior temporal sulcus of the macaque," *Journal of Neurophysiology*, vol. 46, no. 2, pp. 369–384, 1981.

[6] D. N. Pandya and C. Barnes, "Architecture and connections of the frontal lobe," in *The Frontal Lobes Revisited*, E. Perecman, Ed., pp. 41–72, IRBN Press, New York, NY, USA, 1987.

[7] J. M. Hillis, M. O. Ernst, M. S. Banks, and M. S. Landy, "Combining sensory information: mandatory fusion within, but not between, senses," *Science*, vol. 298, no. 5598, pp. 1627–1630, 2002.

[8] D. G. Pelli, "Uncertainty explains many aspects of visual contrast detection and discrimination.," *Journal of the Optical Society of America A*, vol. 2, no. 9, pp. 1508–1532, 1985.

[9] B. A. Dosher, G. Sperling, and S. A. Wurst, "Tradeoffs between stereopsis and proximity luminance covariance as determinants of perceived 3D structure," *Vision Research*, vol. 26, no. 6, pp. 973–990, 1986.

[10] N. V. S. Graham, *Visual Pattern Analyzers*, Oxford University Press, New York, NY, USA, 1989.

[11] C. R. Lin and M. Gerla, "Adaptive clustering for mobile wireless networks," *IEEE Journal on Selected Areas in Communications*, vol. 15, no. 7, pp. 1265–1275, 1997.

[12] A. Iwata, C.-C. Chiang, G. Pei, M. Gerla, and T.-W. Chen, "Scalable routing strategies for ad hoc wireless networks," *IEEE Journal on Selected Areas in Communications*, vol. 17, no. 8, pp. 1369–1379, 1999.

[13] T.-C. Hou and T.-J. Tsai, "An access-based clustering protocol for multihop wireless ad hoc networks," *IEEE Journal on Selected Areas in Communications*, vol. 19, no. 7, pp. 1201–1210, 2001.

[14] C. E. Perkins, "Cluster-based networks," in *Ad Hoc Networking*, C. E. Perkins, Ed., chapter 4, pp. 75–138, Addison-Wesley, Reading, Mass, USA, 2001.

[15] "NET-SENTRIC surveillance," ONR BAA 07-017, http://www.onr.navy.mil/02/baa.

[16] P. Withington, H. Fluhler, and S. Nag, "Enhancing homeland security with advanced UWB sensors," *IEEE Microwave Magazine*, vol. 4, no. 3, pp. 51–58, 2003.

[17] J. M. Mendel, *Uncertain Rule-Based Fuzzy Logic Systems*, Prentice-Hall, Upper Saddle River, NJ, USA, 2001.